SSD-TDR-64-77

2 of 3

50-P $1.25

Breakdown in Waveguides Due to the Multipactor Effect

MAY 1964

Prepared by H. M. WACHOWSKI
Tracking and Radar Department
Sensing and Information Systems Subdivision
Electronics Division

Prepared for COMMANDER SPACE SYSTEMS DIVISION
AIR FORCE SYSTEMS COMMAND
LOS ANGELES AIR FORCE STATION
Los Angeles, California

EL SEGUNDO TECHNICAL OPERATIONS • AEROSPACE CORPORATION
CONTRACT NO. AF 04(695)-269

SSD-TDR-64-77

Report No.
TDR-269(9990)-5

BREAKDOWN IN WAVEGUIDES DUE TO THE MULTIPACTOR EFFECT

Prepared by

H. M. Wachowski
Tracking and Radar Department
Sensing and Information Systems Subdivision
Electronics Division

El Segundo Technical Operations
AEROSPACE CORPORATION
El Segundo, California

May 1964

Contract No. AF 04(695)-269

Prepared for

COMMANDER SPACE SYSTEMS DIVISION
UNITED STATES AIR FORCE
Inglewood, California

SSD-TDR-64-77

Report No.
TDR-269(9990)-5

BREAKDOWN IN WAVEGUIDES DUE TO THE MULTIPACTOR EFFECT

Prepared by:

H. M. Wachowski
H. M. Wachowski
Tracking and Radar Department

This technical documentary report has been reviewed and is approved for publication and dissemination. The conclusions and findings presented herein do not necessarily represent an official Air Force position.

For Aerospace Corporation

N. F. Riordan
N. F. Riordan, Head
Tracking and Radar Department
Sensing and Information Systems
Subdivision, Electronics Division

For Space Systems Division
Air Force Systems Command

Raymond Maloney, Maj. USAF

El Segundo Technical Operations
AEROSPACE CORPORATION
El Segundo, California

ABSTRACT

This report presents the theory of the multipactor effect and applies it to the problem of transmitting high power levels through waveguides operating at low gas pressures. The multipactor effect is a secondary electron resonance phenomenon. As such, it can occur only for certain combinations of operating conditions. Charts are presented showing the operating conditions which lead to the multipactor effect in its various modes. It is shown that only the high order breakdown modes are of concern for ordinary waveguide operation. The theory shows that breakdown in the higher order modes is possible only for certain very restricted ranges of peak voltage. Therefore, it is quite unlikely that multipactor breakdown will actually occur in an ordinary rectangular waveguide. Since published experimental measurements of the multipactor breakdown conditions agree very well with the theory presented here, this theory can be used with a high degree of confidence in making predictions of multipactor breakdown possibilities.

El Segundo Operations
AEROSPACE CORPORATION
El Segundo, California

CONTENTS

FIGURES

SECTION 1

INTRODUCTION

An important design consideration in systems utilizing hollow waveguides operating at low gas pressures and high RF power levels is the prevention of breakdown due to the so-called multipactor effect, or secondary electron resonance. The multipactor effect becomes the dominant high-frequency breakdown mechanism for pressures at which the mean free path of a free electron exceeds the spacing between the broad walls of a rectangular waveguide operating in the dominant TE_{01} mode.

A brief qualitative description of the multipactor effect starts with the assumption that there are a few free electrons present in a waveguide filled with gas at a low pressure. Under the influence of the applied RF electric field, practically every electron crosses the guide without colliding with a gas molecule. Upon striking the waveguide wall, secondary electrons are emitted with a certain statistical probability. For most materials the secondary emission yield (i.e., the total number of emitted secondary electrons per unit time, divided by the total number of incident electrons per unit time) becomes greater than unity if the impact energy of the incident electrons is sufficiently high. If the transit time of an electron across the guide is equal to one-half the period of an RF cycle (or, more generally, any odd multiple of a half-period), then the number of electrons crossing back and forth in synchronism with the applied RF field increases very rapidly in avalanche fashion. Further transmission of RF energy is disrupted as a result.

After a brief discussion of previous investigations of the multipactor effect in Section 2, Sections 3 and 4 present the detailed theory of the multipactor effect. This theory is freely drawn from the published work of K. Krebs and his co-workers in Germany. Of the analytical work published to date on this effect, the work of Krebs and his co-workers stands out as the most complete

and the most nearly free of simplifying assumptions. A brief discussion of experimental results follows in Section 5, after which a series of calculations appropriate to high-power waveguide operation is presented in Section 6. Some conclusions are discussed in Section 7.

SECTION 2

SUMMARY OF PREVIOUS INVESTIGATIONS OF THE MULTIPACTOR EFFECT

The multipactor effect was first investigated by Farnsworth (Ref. 1) who proposed using it to achieve electron beam amplification, an application for which more convenient techniques have since been developed. However, the multipactor effect has become an important consideration in the microwave range of frequencies. Certain power losses in transit-time tubes have been traced to this effect (Refs. 2, 3, and 4). The utilization of this effect to achieve voltage stabilization or power limiting in an RF circuit has been proposed (Ref. 5). Another application which has been investigated is frequency multiplication, since the multipactor current has a high harmonic content (Ref. 6). The extremely rapid buildup of the multipactor effect makes it attractive for duplexing and switching applications (Ref. 7).

Considerable work has been done on the purely analytical and experimental aspects of the multipactor effect. A simplified theory was worked out in 1948 by Gill and von Engel (Ref. 8), who also presented some experimental results. Their theory suffers from the unrealistic assumption that the velocity of emission and the velocity of impact for electrons participating in the multipactor effect have a constant ratio. Two later papers by Hatch and Williams (Refs. 9 and 10) are based on this theory of Gill and von Engel and present more extensive calculations and experimental results. Probably the most extensive and careful investigations of the multipactor effect have been those carried out by K. Krebs and his co-workers in Germany. In an analytical paper published in 1955 (Ref. 11), Krebs and Meerbach presented a one-dimensional analysis of the multipactor effect between parallel planes. The analysis, which is free from the unrealistic assumption made by Gill and von Engel, is worked out in painstaking detail and forms the basis for all of the later papers of Krebs. The velocity distribution and density of the secondary

electrons were investigated experimentally and reported in a paper published in 1956 (Ref. 12). Investigations of frequency multiplication by means of the multipactor effect were published by Krebs in 1959 (Ref. 6). The excitation of resonators by the multipactor current was also described in a separate paper (Ref. 13). Extensive experimental investigations in the decimeter wavelength range were published in 1962 (Ref. 14). A recent paper by Krebs and Kossel (Ref. 15) presents additional experimental results, which provide additional confirmation of the theory presented in the 1955 paper (Ref. 11). In some fundamental respects the predictions of this theory differ essentially from corresponding predictions based upon the theory of Gill and von Engel. The difference is due to the less restrictive initial assumptions, and experimental results to a large extent confirm the validity of the analysis of Krebs and Meerbach. This analysis will, therefore, be used as the basis for discussion in the remainder of this report.

SECTION 3

ONE-DIMENSIONAL ANALYSIS OF THE MULTIPACTOR EFFECT

3.1 THE DETERMINATION OF BREAKDOWN REGIONS AND ELECTRON ARRIVAL PHASES

It is assumed that a homogeneous RF electric field of angular frequency ω is applied between two parallel plates whose secondary emission ratio, which is a function of the impact energy of the incident electrons, becomes greater than unity for sufficiently large values of impact energy. The spacing between plates is denoted by a, the peak field intensity by U_0/a, and the x coordinate is measured normal to the plates U_0 is the peak voltage across the plates. In the case of a rectangular waveguide operating in the dominant TE_{01} mode, the electric field is everywhere in the direction normal to the broad walls of the guide. Its amplitude varies sinusoidally across the guide, having its maximum value at the center of the guide and falling to zero at both narrow side walls. Hence, a free electron in a hollow guide will be accelerated by the electric field in a direction normal to the broad walls and a one-dimensional theory will be sufficient. Figure 1 illustrates the geometry of the problem and shows qualitatively several different electron trajectories for different emission phases. These will be discussed in connection with the analysis to be presented.

To determine multipactor starting conditions, it is sufficient to focus attention on a single electron moving under the influence of the applied RF electric field. The time t_0 at which this electron is emitted from one plate and the time t_A at which it arrives at the opposite plate correspond to the phase angles $\phi_0 = \omega t_0$ and $\phi_A = \omega t_A$, respectively. The equation of motion of the electron is

$$\ddot{x} = \frac{e}{m} \frac{U_0}{a} \sin \omega t \qquad (1)$$

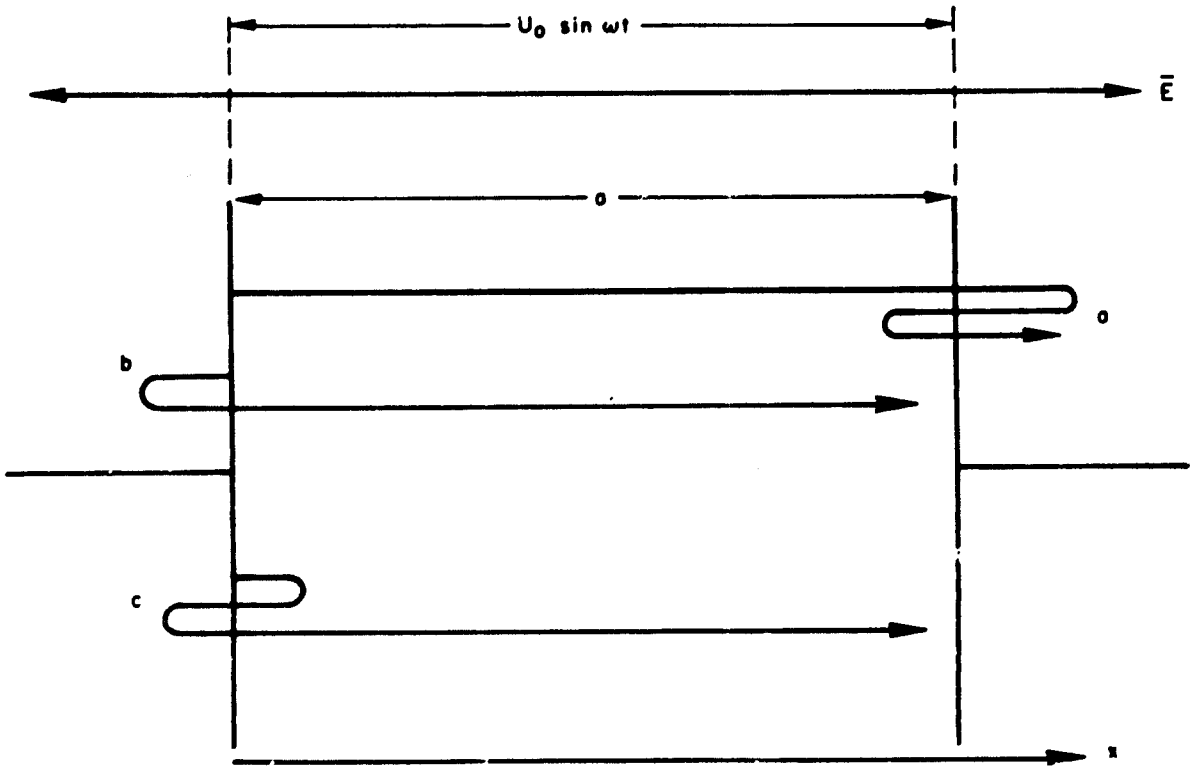

Figure 1. Electron Trajectories Between Parallel Plates (from Annalen der Phy ik, Band 15, 1955, p. 190)

A first integration yields

$$\dot{x} = \int_{t_0}^{t} \ddot{x}\, dt + v_s = \frac{e}{m}\,\frac{U_0}{\omega a}(\cos\phi_0 - \cos\phi) + v_s \qquad (2)$$

where e and m are the charge and mass of the electron ($e/m = 1.76 \times 10^{11}$ coulomb/kg), v_s is the velocity of emission of the electron, and the phase $\phi = \omega t$ replaces the time t as the variable. In reality, secondary electrons are emitted with a velocity distribution which peaks at electron energies of a few electron volts. The characteristics of the distribution vary with the emitting material and the impact energy of the incident electrons (Refs. 16 and 17). In this analysis, a definite value v_s is assumed for the emission velocity, which one may interpret as the most probable value. The assumption of a velocity distribution would seriously complicate the analysis.

Integrating Eq. (2) for one complete traversal of the guide yields

$$a = \int_{t_0}^{t_A} \dot{x}\, dt = \int_{\phi_0}^{\phi_A} \frac{\dot{x}}{\omega}\, d\phi = \left(\frac{eU_0}{m\omega^2 a}\cos\phi_0 + \frac{v_s}{\omega}\right)(\phi_A - \phi_0) - \frac{eU_0}{m\omega^2 a}(\sin\phi_A - \sin\phi_0) \qquad (3)$$

At this point Krebs and Meerbach introduce dimensionless ratios, which permit subsequent computed results to apply to a wide variety of cases. The quantities U_s and U^* (having the dimensions of voltage) are defined as

$$U_s = \frac{1}{2}\,\frac{m}{e}\,v_s^2 \qquad (4)$$

$$U^* = \frac{m\omega^2 a^2}{e} \qquad (5)$$

and the dimensionless ratios β and γ are defined as

$$\beta = \frac{U_0}{U^*} \tag{6}$$

$$\gamma = \frac{U_s}{U^*} \tag{7}$$

Equation (3) may now be rewritten as

$$) = (\beta \cos \phi_0 + \sqrt{2\gamma})(\phi_A - \phi_0) - \beta(\sin \phi_A - \sin \phi_0) \tag{8}$$

where all quantities are now dimensionless. This equation implicitly yields the arrival phase ϕ_A as a function of emission phase ϕ_0 for assumed values of β and γ (i.e., peak RF electric field and initial velocity of emission). The case $\gamma = 0$ was computed by Krebs and Meerbach for various values of β. Their results are reproduced in Figure 2. The normalizing voltage U^* can be expressed as

$$\begin{aligned} U^* &= 2.020 \times 10^7 \left(\frac{a}{\lambda}\right)^2 \text{volts} \\ &= 2.244 \times 10^{-2} (f\,a)^2 \text{volts} \quad (f \text{ in Mc, } a \text{ in cm}) \end{aligned} \tag{9}$$

Figure 2 shows that ϕ_A has solutions even in the region from $\phi_0 = 0$ to $\phi_0 = -\pi/2$, when the emitted electron experiences a force that drives it back toward the emitting surface. Furthermore, for certain ranges of value of ϕ_0 the corresponding solution for ϕ_A is multiple-valued. Both of these circumstances are due to the implicit assumption that the applied field exists for all values of x, and that the planes $x = 0$ and $x = a$ act as ideal grids permitting electrons to flow past these planes. The multiple-valued solutions for ϕ_A

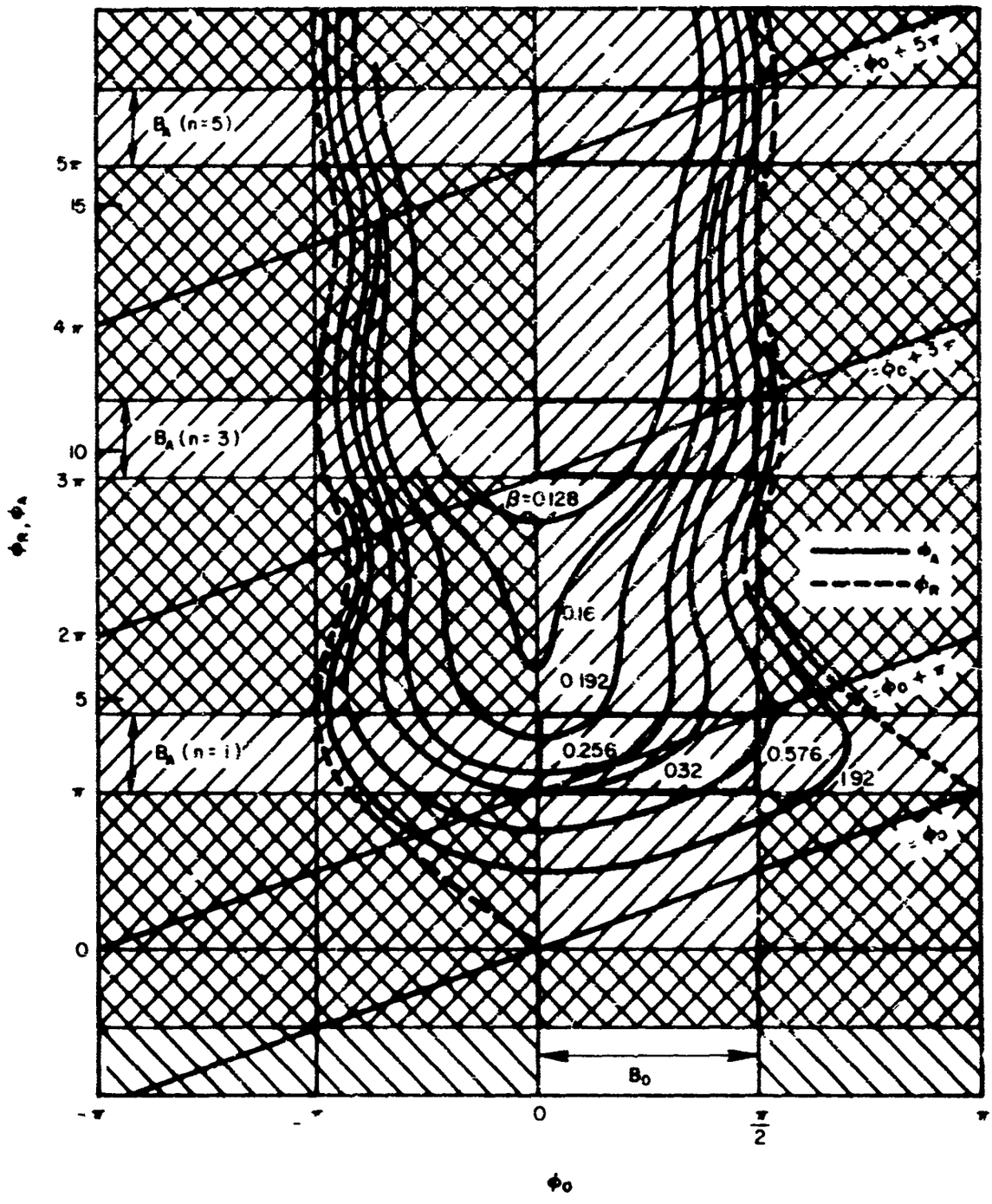

Figure 2. Arrival and Return Phases, ϕ_A and ϕ_R, for $\gamma = 0$
(from Annalen der Physik, Band 15, 1955, p. 191)

correspond physically to an electron which oscillates about the position of the arrival plane x = a (trajectory a in Figure 1). An electron that is emitted between $\phi_0 = -\pi/2$ and $\phi_0 = 0$ has an initial negative acceleration and reaches the opposite wall only after passing the starting plane x = 0 once more (trajectory b in Figure 1). In order for an electron to actually reach the opposite wall, one of the following two conditions must be fulfilled, where ϕ_R denotes the phase angle at which a hypothetical electron following a trajectory of type b in Figure 1 returns to the starting plane x = 0:

$$\left.\begin{array}{l} \phi_A \text{ real, } \phi_R \text{ not real} \\ \\ \phi_A \text{ and } \phi_R \text{ real, with } \phi_R > \phi_A \end{array}\right\} \qquad (10)$$

The first of these two possibilities corresponds to an electron which leaves the plane x = 0 and is drawn to the opposite plane x = a without returning to x = 0, either before or after the time of arrival at x = a. The second corresponds to an electron which leaves x = 0, reaches x = a without returning to x = 0, but, due to the fact that this mathematical formulation allows electrons to pass freely through the planes x = 0 and x = a, reaches x = 0 again at a later time. In reality, whenever an electron reaches either of the planes x = 0 and x = a, it impacts against a solid wall and its trajectory is thereby terminated. The case when ϕ_A and ϕ_R are both real with $\phi_R < \phi_A$ must be excluded here on physical grounds, since this case corresponds to an electron which returns to the plane x = 0 one or two times (trajectories b and c in Figure 1) before crossing to the plane x = a. The trajectory would, of course, end upon the first return to x = 0.

Thus, consideration of the return phase ϕ_R is essential to an understanding of the multipactor effect. An equation relating ϕ_R to ϕ_0 may be obtained by setting a = 0 and replacing ϕ_A by ϕ_R in Equation (3). The result is:

$$\left(\cos\phi_0 + \frac{\sqrt{2\gamma}}{\beta}\right)\phi_R - \sin\phi_R = \left(\cos\phi_0 + \frac{\sqrt{2\gamma}}{\beta}\right)\phi_0 - \sin\phi_0 \qquad (11)$$

Using this equation, Krebs and Meerbach have computed corresponding pairs of values ϕ_R and ϕ_0 for various values of the parameter $\sqrt{2\gamma}/\beta$. The results are given in Figure 3. It can be seen that there are two values (1.10 and 1.26) of $\sqrt{2\gamma}/\beta$ for which the solution of Equation (11) consists of a single point instead of a contour. For values

$$\sqrt{2\gamma}/\beta > 1.26 \tag{12}$$

there exist no real solutions for ϕ_R, regardless of the starting phase ϕ_0. This is easy to understand, since for small values of applied electric field (i.e., small values of β) the initial velocity v_s of an electron becomes relatively more important. For a sufficiently high value of v_s (namely, a value for which $\sqrt{2\gamma}/\beta > 1.26$) the electron does not return to the plane $x = 0$, regardless of the starting phase ϕ_0. Equation (11) also has the trivial solution $\phi_R = \phi_0$ for all values of $\sqrt{2\gamma}/\beta$. This solution is meaningless and is disregarded.

The $\gamma = 0$ curve of Figure 3 is drawn in Figure 2 as the dashed curve. The lower limit of the range of ϕ_0 within which multipactor breakdown can occur is $\phi_0 = 0$, since for $\phi_0 < 0$ there are solutions for ϕ_R such that $\phi_R < \phi_A$, violating conditions (10). Physically, this corresponds to the fact that an electron with zero initial velocity at the plane $x = 0$ will be drawn toward negative values of x if $\phi_0 < 0$. The upper limit of the breakdown range of ϕ_0 for $\beta < \sim 0.5$ is $\phi_0 = \pi/2$. For $\phi_0 > \pi/2$ and $\beta > \sim 0.5$, Figure 2 shows that there are solutions $\phi_R > \phi_A$. In general, then, the effective range of ϕ_0 is a function of β (i.e., applied RF electric field intensity). This effective range will be further restricted by considerations of phase focusing to be discussed in Section 3.2.

As discussed in Section 1, in order to initiate multipactor breakdown, an electron must arrive at the plane $x = a$ at a phase ϕ_A which, as seen from the plane $x = a$, lies within an effective range of phase for which newly

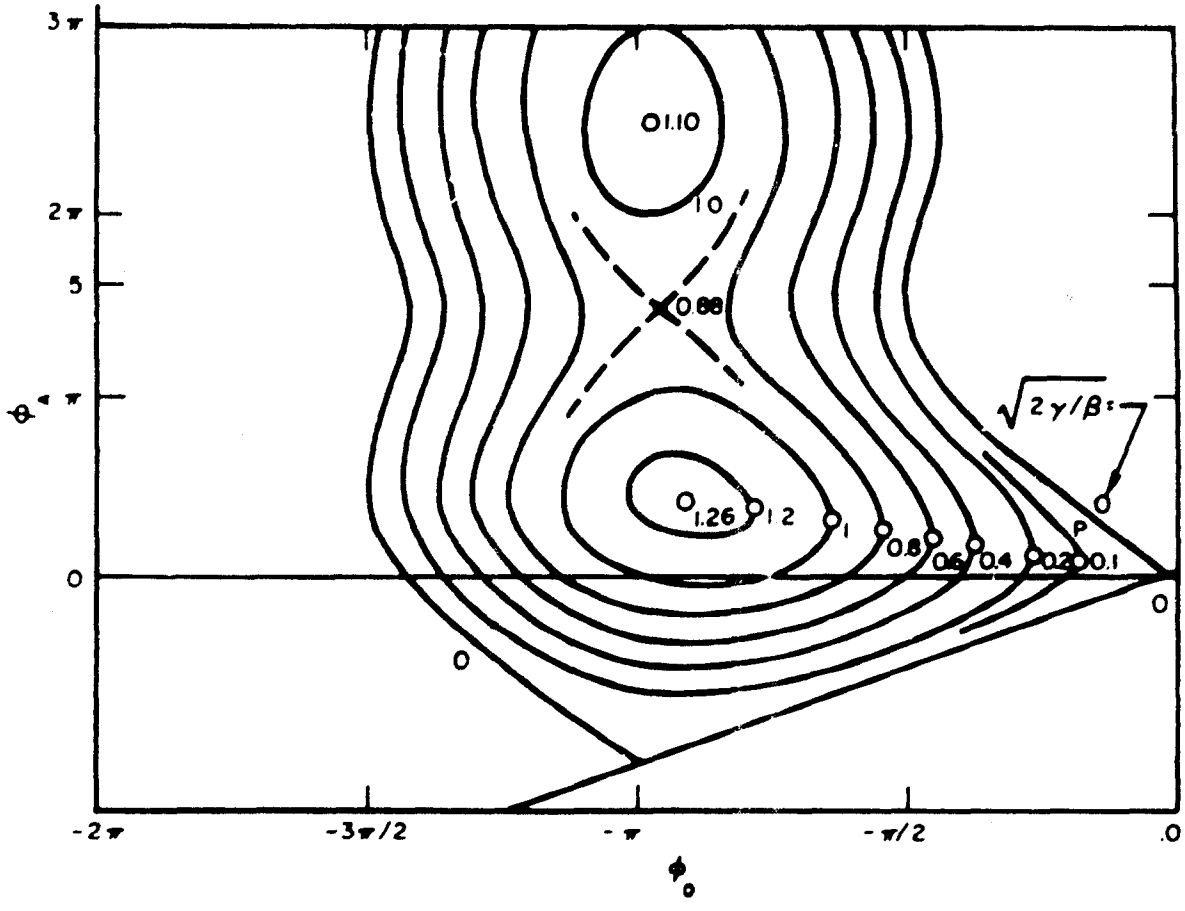

Figure 3. Return Phase ϕ_R for Various Values of the Parameter $\sqrt{2\gamma}/\beta$ (from Annalen der Physik, Band 15, 1955, p. 193)

emitted electrons will reach the plane x = 0. Thus, the effective ranges of arrival phase ϕ_A, denoted by B_A in Figure 2, are simply the effective range of departure phase ϕ_0, denoted by B_0, displaced by odd multiples of π. Thus,

$$B_A = B_0 + n\pi \qquad n = 1, 3, 5, \ldots$$

In Figure 2, the boundaries of the ranges B_A are given by the intersection of the boundaries of B_0 with the straight lines $\phi_A = \phi_0 + n\pi$. The regions of interest for the multipactor effect are the rectangular areas in Figure 2 which have been left without cross-hatching (drawn for $\beta < \sim 0.5$).

A computed example for a case when $\gamma \neq 0$ is given in Figure 4. The values assumed are $\gamma = 6.4 \times 10^{-3}$ and $\beta = 0.32$, corresponding (for a value $U^* = 1000$ volts) to an emission energy of 6.4 electron volts and a peak RF voltage of 320 volts. For the case of an X-band waveguide, U^* is in the neighborhood of 2×10^6 volts, which would yield extremely small values of γ and β, even for high-power operation. However, returning to the computed case of Krebs and Meerbach, the effect of the non-zero initial velocity is to shift the lower limit of the effective range of ϕ_0 to a value $\phi_C \approx -1$, as can be seen from Figure 4. Thus, for $-1 < \phi_0 < 0$, when a retarding field is applied, an electron with 6.4 electron volts of energy at emission still reaches the plane x = a without returning to the plane x = 0. For $\phi_0 < -1$, the electron would be drawn backward to negative values of x, and then pass the plane x = 0 once more before reaching the plane x = a. Thus, for such a value of ϕ_0 there exist two solutions $\phi_R < \phi_A$ (trajectory c in Figure 1). In reality, such an electron would have its trajectory terminated at the first return to x = 0. The upper boundary of the effective range of ϕ_0 is given by that value at which the ϕ_R curve becomes tangent to the vertical, in the present case at a value of ϕ_0 slightly in excess of $\pi/2$.

The critical values ϕ_{0k} of the starting phase ϕ_0 at which the ϕ_R curve becomes tangent to the vertical have been computed as a function of the parameter

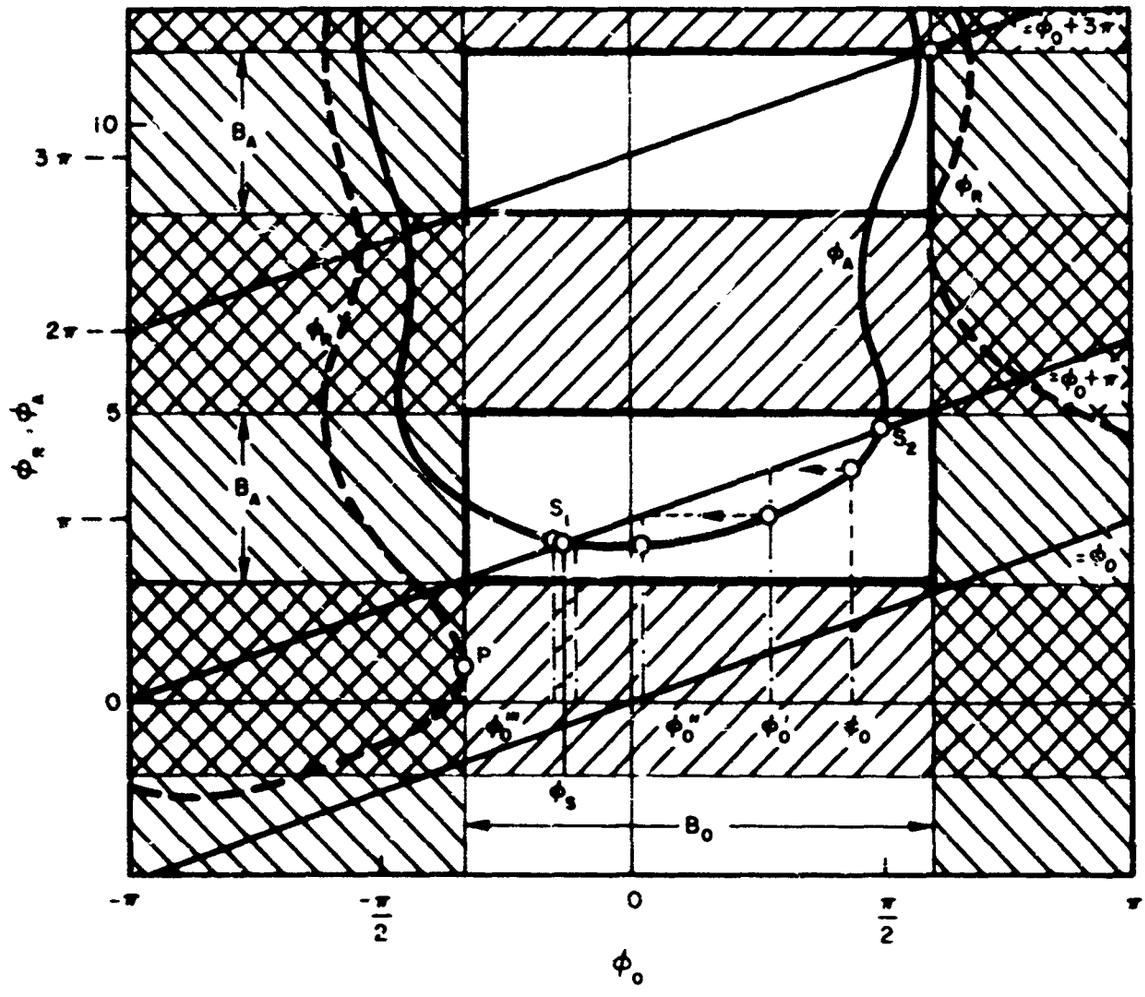

Figure 4. Arrival and Return Phases ϕ_A and ϕ_R for $\beta = 0.32$ and $\gamma = 0.0064$; Effective Breakdown Regions and the Principle of Phase Focusing are Illustrated (from Annalen der Physik, Band 15, 1955, p. 193)

$\beta/\sqrt{2\gamma}$ and are plotted in Figure 5. For the case of large values of $\beta/\sqrt{2\gamma}$, ϕ_{0k} approaches the limiting value

$$\phi_{0k} = -\sqrt{\frac{8}{3}\frac{\sqrt{2\gamma}}{\beta}} \tag{13}$$

3.2 PHASE FOCUSING

As seen from the plane x = a, the starting phase ϕ_0' of a secondary electron is effectively related to the arrival phase of the corresponding primary electron as seen from the plane x = 0 by a simple phase reversal due to the reversal in direction of travel of the secondary electron as compared to the arriving primary electron:

$$\phi_0' = \phi_A - n\pi \qquad n = 1, 3, 5, \ldots \tag{14}$$

The starting phase ϕ_0' is conveniently obtained graphically on Figure 4 by projecting the arrival phase ϕ_A horizontally on the straight line $\phi_0 + n\pi$. By repeating this process, a series of successive starting phases ϕ_0, ϕ_0', ϕ_0'', ϕ_0''', . . . is obtained, based upon the starting phase ϕ_0 of the original electron assumed to be $4\pi/9$ in the example of Figure 4. The successive starting phases correspond to the successive traversals of the interelectrode space by the descendants of the original electron. A series of starting phases is obtained which approaches the point S_1 (the intersection of the ϕ_A vs ϕ_0 curve with the straight line $\phi_0 + \pi$) corresponding to the phase designated as ϕ_s. The point S_1 is said to be "phase pure"; electrons starting at this phase from either of the planes x = 0 and x = a reach the opposite plane at the same phase ϕ_s, as seen from the opposite plane. This, then, is the phase about which phase focusing takes place. A bunching occurs whereby the electrons form themselves into a sheet of charge which crosses back and forth between x = 0 and x = a with ever-increasing density, leading to multipactor breakdown. The center of the sheet always leaves either plane at the phase ϕ_s. In

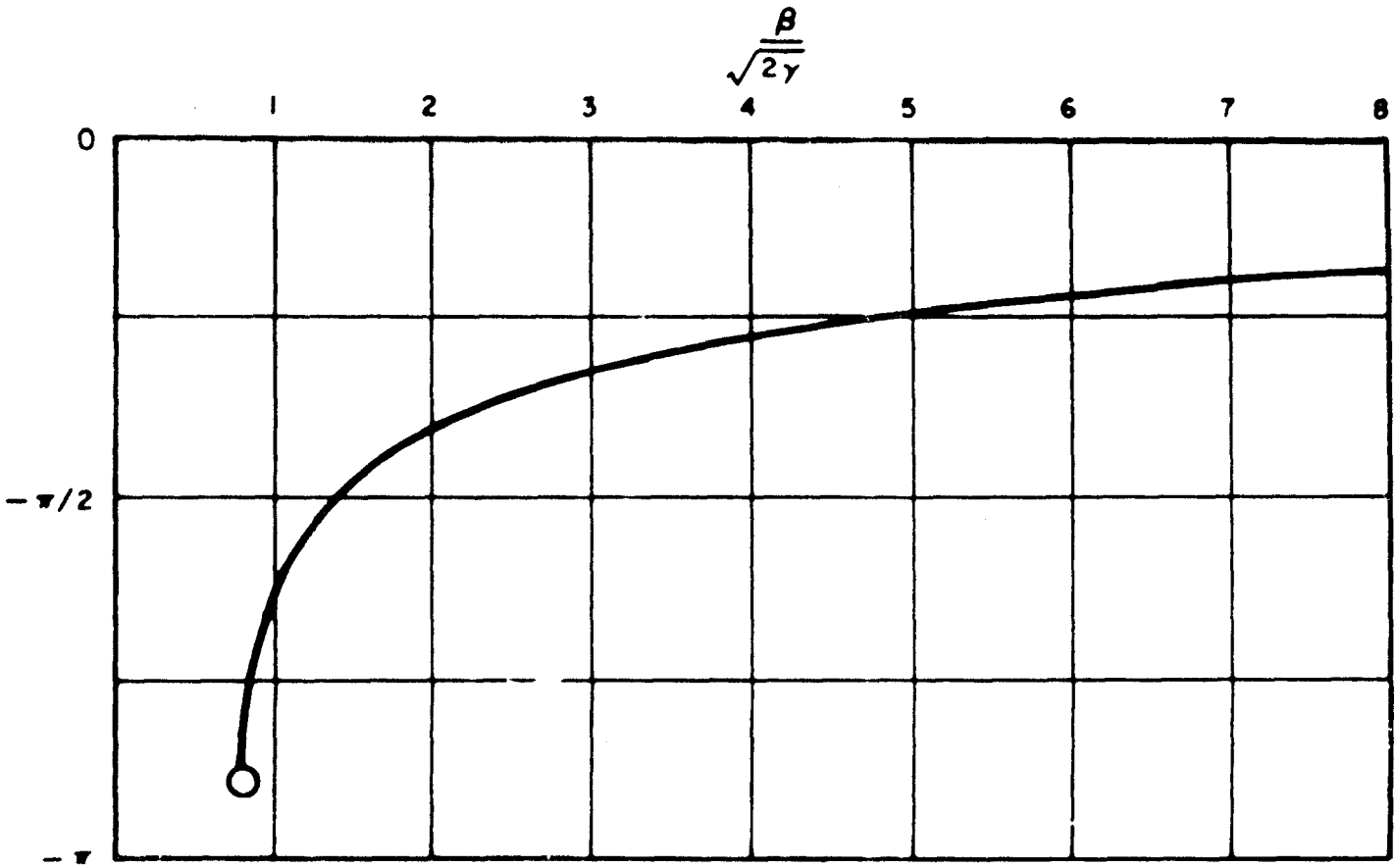

Figure 5. Critical Values ϕ_{0k} of Starting Phase as a Function of $\beta/\sqrt{2\gamma}$ (from Annalen der Physik, Band 15, 1955, p. 194)

the case of a higher-order multipactor mode, there will be more than one sheet simultaneously present between the electrodes.

It may easily be seen that the second intersection point, S_2, is also phase pure. However, the corresponding starting phase is not stable; an electron starting at a phase deviating slightly from this phase will result in later secondary electrons with a succession of starting phases which diverge from the phase corresponding to the point S_2. Successive starting phases will sooner or later end up either at point S_1 or in an ineffective range of ϕ_0. This can be seen by applying the same graphical procedure again.

In practical cases, it can be shown that an ineffective range of ϕ_0 will always exist. According to Equation (2), making use of the definitions of Equations (4), (5), (6), and (7), the arrival or impact velocity v_A is given by

$$v_A = \dot{x}_{(\phi=\phi_A)} = v_s\left[\frac{\beta}{\sqrt{2\gamma}}(\cos\phi_0 - \cos\phi_A) + 1\right] \tag{15a}$$

or, expressed in electron volts,

$$U_A = U_s\left[\frac{\beta}{\sqrt{2\gamma}}(\cos\phi_0 - \cos\phi_A) + 1\right]^2 \tag{15b}$$

Thus, small values of $\beta/\sqrt{2\gamma}$ correspond to small values of impact energy. However, the impact energy must be sufficiently high to assure that the secondary emission ratio δ will exceed unity. Minimum impact energies of the order of 100 eV are required for most metals. The emission velocity of the secondary electrons is assumed to have an average value corresponding to 10 eV. The term $(\cos\phi_0 - \cos\phi_A)$ can assume a maximum value of 2. Making these substitutions into Equation (15b) yields

$$10\left[\frac{2\beta}{\sqrt{2\gamma}} + 1\right]^2 \gtrsim 100 \tag{16}$$

leading to the following requirement for $\beta/\sqrt{2\gamma}$:

$$\frac{\beta}{\sqrt{2\gamma}} \gtrsim 1 \tag{17}$$

in order that multipactor breakdown can occur at all. However, according to Equation (12) and Figure 3, ineffective ranges of ϕ_0 cease to exist only for $\beta/\sqrt{2\gamma} < 1/1.26 \approx 0.8$. Thus, in actual cases of multipactor breakdown, ineffective ranges of ϕ_0 always exist.

The criterion for stability of a phase pure point can be expressed in terms of the slope of the ϕ_A curve at such a point. Only those phase pure points are stable for which

$$\left|\frac{d\phi_A}{d\phi_0}\right| < 1 \tag{18}$$

A multipactor breakdown will take place about the phase ϕ_s corresponding to such a point. For the onset of this breakdown, only a single electron is initially necessary. For the maintenance of the breakdown the extent of the range of ϕ_0 that is focused to the phase ϕ_s is unimportant. To compute the phase pure points ϕ_s as a function of β and γ, the substitutions $\phi_0 = \phi_s$ and $\phi_A = \phi_s + n\pi$ are made in Equation (8), yielding

$$1 = (\beta \cos \phi_s + \sqrt{2\gamma})n\pi + 2\beta \sin \phi_s \tag{19}$$

This is then solved for ϕ_s:

$$\phi_s = \pm \arccos \frac{1}{\beta} \frac{(1 - n\pi\sqrt{2\gamma})}{\sqrt{4 + n^2\pi^2}} + \arctan \frac{2}{n\pi} \qquad n = 1, 3, 5, \ldots \tag{20}$$

3.3 IMPACT ENERGY

The impact energy of phase-focused electrons can be obtained from Equation (15b) by setting $\phi_0 = \phi_s$ and $\phi_A = \phi_s + \pi$, and normalizing the result by dividing by the voltage U^* defined in (5) The result is

$$U_A/U^* = \left[\beta\sqrt{2}\cos\phi_s + \sqrt{\gamma}\right]^2 \tag{21}$$

where ϕ_s is given by Equation (20). As discussed in Section 3.2, this impact energy must exceed a certain value of the order of 100 eV in order for the secondary emission ratio δ to exceed unity.

3.4 CRITICAL VOLTAGE AMPLITUDES FOR THE INITIATION AND EXTINCTION OF MULTIPACTOR BREAKDOWN

An alternative graphical presentation of multipactor breakdown regions plotted on γ and β axes is given in Figure 6. The effective region is the area which is free of any diagonal cross-hatching. Contours of constant values of ϕ_s and U_A/U^* are plotted within the effective region. The operating point for a given physical situation is easily obtained on this chart, since a knowledge of a, ω, U_0 and U_s permits the computation of U^*, γ, and β.

In order for phase focusing to take place, ϕ_s determined from Equation (20) must be real-valued, i.e., the argument of the arc cos function must not exceed unity. Thus, phase pure points exist only for sufficiently large values of β. In general, there will then be two values of ϕ_s due to the double sign appearing in Equation (20). The minus sign corresponds to the point S_1 of Figure 4, while the plus sign corresponds to S_2. For the one particular value β_e of β

$$\beta_e = \frac{1 - n\pi\sqrt{2\gamma}}{\sqrt{4 + n^2\pi^2}} \tag{22}$$

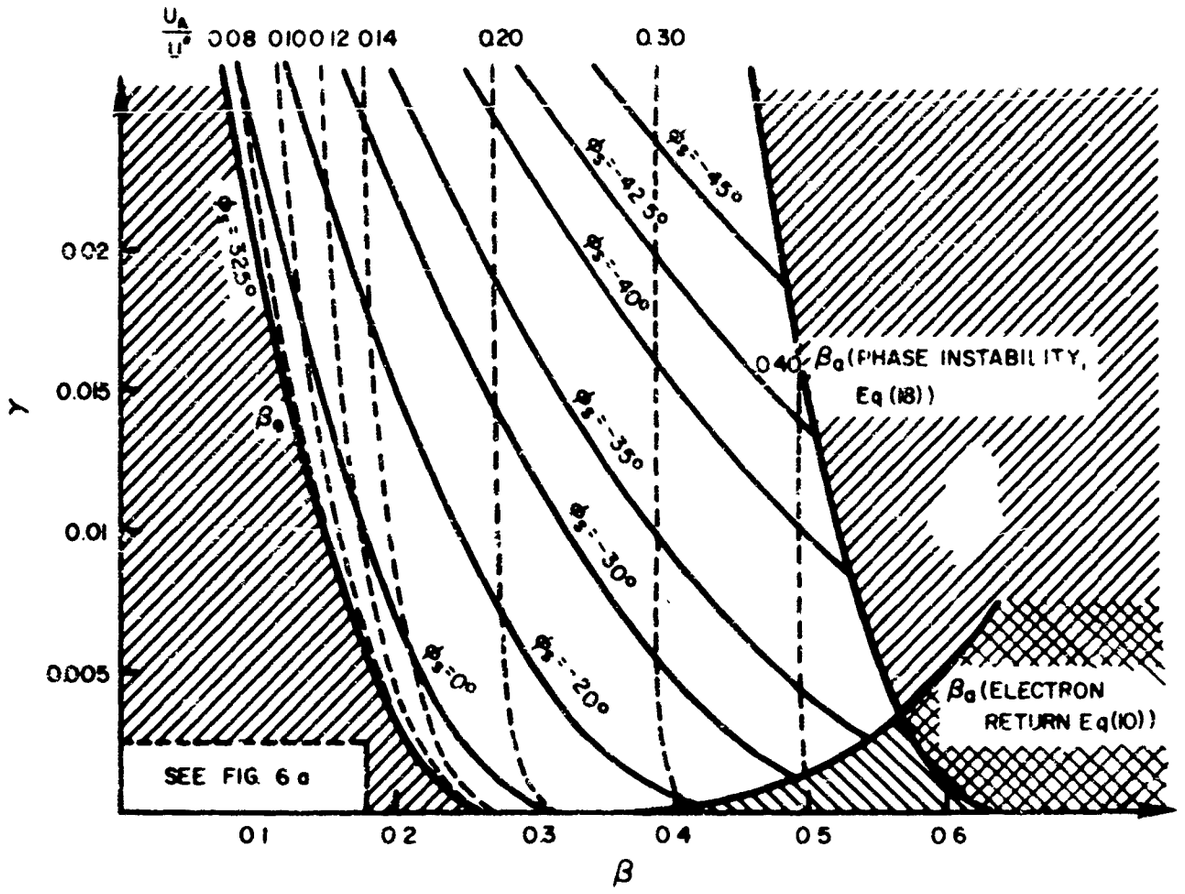

Figure 6. Relative Voltage Amplitudes β_e and β_a for Initiation and Extinction of Multipactor Breakdown
(from Annalen der Physik Band 15, 1955, p. 197)

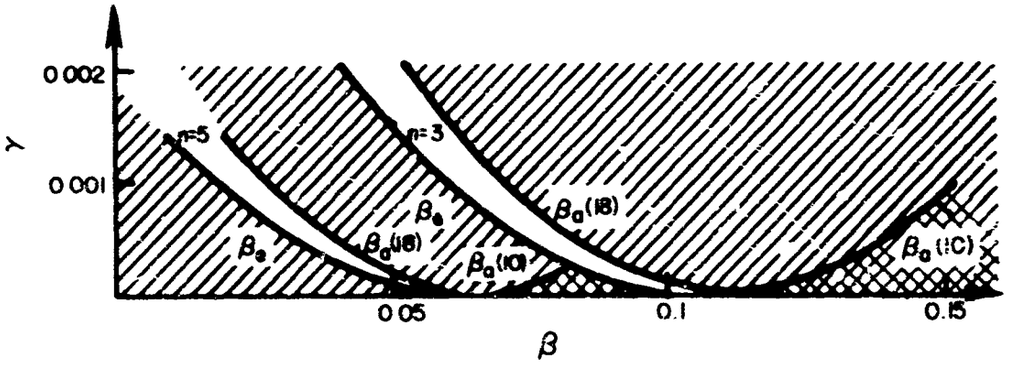

Figure 6a. Enlarged Section of Figure 6, Showing the n = 3 and n = 5 Cases

there is only one solution for ϕ_s, namely, $\phi_s = \arctan(2/n\pi)$. In the representation of Figure 4, the ϕ_A-curve corresponding to this particular value β_e would be tangent to the straight line $\phi_0 + n\pi$. Thus, starting with a low value of voltage amplitude such that $\beta < \beta_e$ no multipactor breakdown can exist until the voltage is increased to the value corresponding to $\beta = \beta_e$ of Equation (22). Breakdown continues for values $\beta > \beta_e$ up to a certain upper limit, which will be investigated in a later paragraph. The critical starting amplitude U_e for the n = 1 mode of breakdown is found from Equation (22) to be, in volts,

$$U_e = \beta_e U^* = 5.43 \times 10^6 \left(\frac{a}{\lambda}\right)^2 \left[1 - 0.99 \times 10^{-3} \frac{\lambda}{a}\sqrt{U_s}\right] \qquad (22a)$$

where U_s is expressed in volts. The critical value β_e of β, given in Equation (22), is plotted for n = 1 in Figure 6 and forms the lower boundary, relative to the β-axis, of the multipactor breakdown region. Of course, breakdown will occur only if, in addition, the impact energy given by Equation (21) is sufficiently great. If the wall material, wall spacing, and frequency are such that the necessary impact energy is attained only for a value of β greater than β_e, then the appropriate contour of constant impact energy in Figure 6 will form the lower boundary of the breakdown region.

The critical starting amplitude U_e for the higher order breakdown modes may be expressed as

$$U_e = \beta_e U^* = \frac{2.020 \times 10^7}{\sqrt{4 + n^2\pi^2}} \left(\frac{a}{\lambda}\right)^2 \left[1 - 0.99 \times 10^{-3} n \frac{\lambda}{a}\sqrt{U_s}\right] \qquad (22b)$$

where U_e and U_s are both in volts, and n is an odd integer. The breakdown regions for the n = 3 and n = 5 modes are shown in Figure 6a.

As β is increased beyond $\beta = \beta_e$, a value is eventually reached at which the breakdown is extinguished. This can be seen from the present analysis As β increases beyond $\beta = \beta_e$, the two phase pure points S_1 and S_2 start from the single phase pure point corresponding to $\beta = \beta_e$ and move apart in opposite directions along the line $\phi_0 + n\pi$. The one really essential point S_1 moves downward and toward the left in the representation of Figure 4 until a particular value $\beta = \beta_a$ is reached for which the starting and arrival phases ϕ_s and ϕ_A of S_1 begin to violate one of the conditions expressed in Equation (10) or Equation (18).

Condition (10) is violated when the starting phase ϕ_s given by Equation (20) becomes equal to the critical value ϕ_{0k} represented in Figure 5. Thus,

$$\phi_{0k} = -\arccos \frac{1}{\beta_a} \frac{(1 - n\pi\sqrt{2\gamma})}{\sqrt{4 + n^2\pi^2}} + \arctan \frac{2}{n\pi} \tag{23}$$

This equation cannot be explicitly solved for β_a, except for $\gamma = 0$, when $\beta_a = 1/n\pi$. A numerical-graphical solution can, however, be obtained and is plotted in Figure 6 as β_a (electron return according to Equation (10)).

To investigate the influence of condition (18), the derivative $d\phi_A/d\phi_0$ is found from differentiation of Equation (8). The substitutions $\phi_0 = \phi_s$, $\phi_a = \phi_s + n\pi$ are made in the result, due to the phase purity of the point S_1. The result is

$$\left(\frac{d\phi_A}{d\phi_0}\right)_{\phi_0=\phi_s} = \frac{n\pi \sin \phi_s + \sqrt{2\gamma}/\beta}{2 \cos \phi_s + \sqrt{2\gamma}/\beta} \tag{24}$$

The critical values $\phi_s = \phi_{sk}$ for which $|d\phi_A/d\phi_0| = 1$ are given by

$$\frac{n\pi \sin \phi_s + \sqrt{2\lambda}/\beta}{2 \cos \phi_s + \sqrt{2\lambda}/\beta} = \pm 1 \tag{25}$$

For the plus sign one obtains

$$\phi_{sk} = \arctan \frac{2}{n\pi} \tag{26}$$

which has the following values:

n =	1	3	5
ϕ_{sk} =	0.564	0.206	0.127
	= 32.5 deg	11.9 deg	7.3 deg

These values correspond to the condition of tangency between the ϕ_A curves of Figures 2 or 4 and the straight lines $\phi_0 + n\pi$, for the slope of the straight lines is unity. No new information is gained here, therefore.

For the minus sign in Equation (25), a critical starting phase is determined for which the phase pure point S_1 becomes unstable for increasing β. Thus, condition (18) is violated when the phase pure starting phase ϕ_s given by Equation (20) becomes equal to the critical value ϕ_{sk} given by Equation (25) with the minus sign. Setting the two expressions equal to each other, one obtains after some algebraic manipulation the result

$$\beta = \beta_a = \sqrt{\left(\sqrt{2\gamma} - \frac{n\pi}{n^2\pi^2 - 4}\right)^2 + \left(\frac{2}{n^2\pi^2 - 4}\right)^2} \tag{27}$$

which is plotted in Figure 6 as β_a (instability of ϕ_s according to Equation (18)).

Figure 6 shows that for the case n = 1 (electron crossing in one-half cycle) a relatively large effective amplitude range exists. Especially remarkable is the rapid increase in this range as the assumed emission velocity increases from zero.

The higher-order breakdown modes (n = 3, 5, . . .) are possible only in relatively restricted amplitude ranges, which also depend in a sensitive way upon the assumed value of emission velocity. The velocity distribution of the secondary electrons, which has been neglected in this analysis, will make the existence of higher-order breakdown modes quite unlikely, since Figure 6 shows that different velocities of emission (such as exist in a velocity distribution) will correspond to different effective amplitude ranges. Thus, only a small fraction of the emitted electrons may fall within the effective range of γ for a given β. Moreover, the smaller values of β appropriate to the higher-order modes lead to smaller impact energies according to Equation (21), often eliminating the breakdown possibility.

The consequences of varying parameters other than U_0 can also be determined by the diagram of Figure 6. Changing either a or ω while holding all other parameters constant will change U^* according to Equation (5), which will change γ and β by a common multiplicative factor. Hence, the operating point in Figure 6 will move along an inclined straight line passing through the origin.

SECTION 4

ALTERNATE REPRESENTATIONS OF BREAKDOWN CONDITIONS

The breakdown conditions can be portrayed in still other ways which are convenient for certain purposes. Figure 7, taken from Reference 6, represents the starting phase ϕ_s of the phase pure points as a function of β for varying values of γ. Only the solid portions of the curves enclosed by the dotted curves are of significance. The dotted curves represent the limiting conditions on phase focusing and electron reflection represented by Equations (18) and (10). Only the n = 1 mode is plotted here. Still another representation, which for practical applications is perhaps the most useful, portrays existence regions for the multipactor effect plotted on axes representing, respectively, peak RF voltage U_o and the product af of wall spacing a and operating frequency f. Such a representation is given in Figure 8, computed for an emission energy of 5 eV. The critical starting amplitude, expressed in terms of a and f, is easily found from Equation (22a) for the n = 1 case:

$$U_e = 6.03 \times 10^{-3}(af)^2 - 0.179(af)\sqrt{U_s} \tag{28}$$

where a is in centimeters, f in Mc, and U_s in volts. Plotted to logarithmic scales, Equation (28) will give a straight line. Corresponding starting amplitudes for the higher order breakdown modes are likewise easily found from Equation (22). The results for the first few higher order modes are:

$$n = 3: \quad U_e = 2.329 \times 10^{-3}(af)^2 - 0.2072(af)\sqrt{U_s} \tag{28a}$$

$$n = 5: \quad U_e = 1.417 \times 10^{-3}(af)^2 - 0.2101(af)\sqrt{U_s} \tag{28b}$$

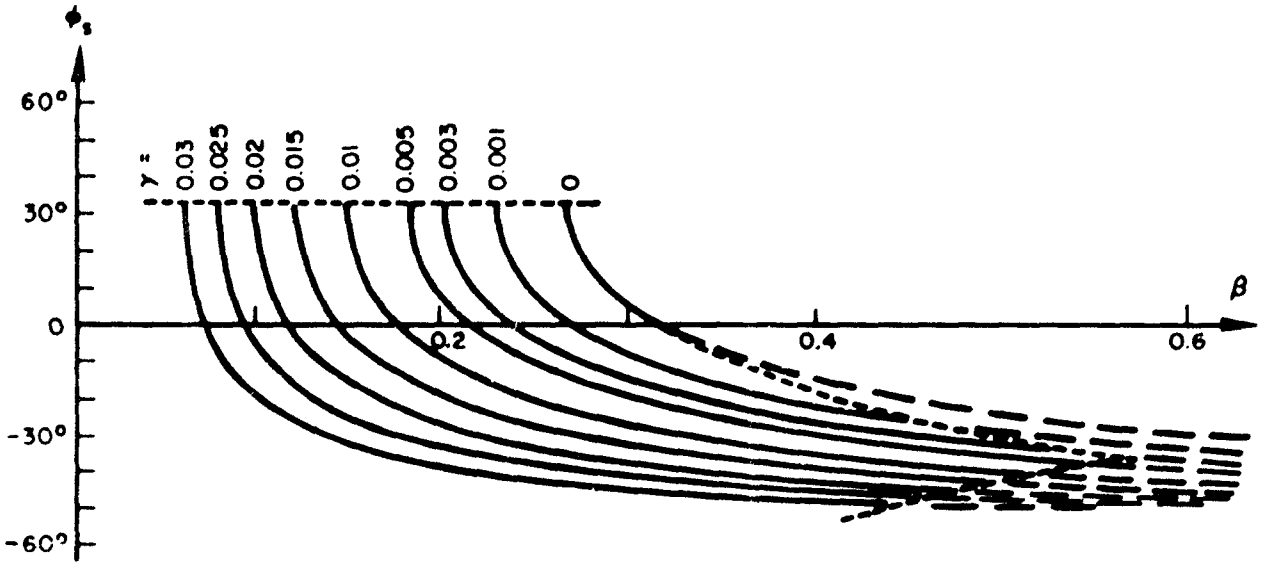

Figure 7. Phase Focus ϕ_s of Secondary Electrons as Function of Voltage Amplitude β and Emission Energy γ (from Zeitschrift für Physik, Band 154, 1959, p. 21)

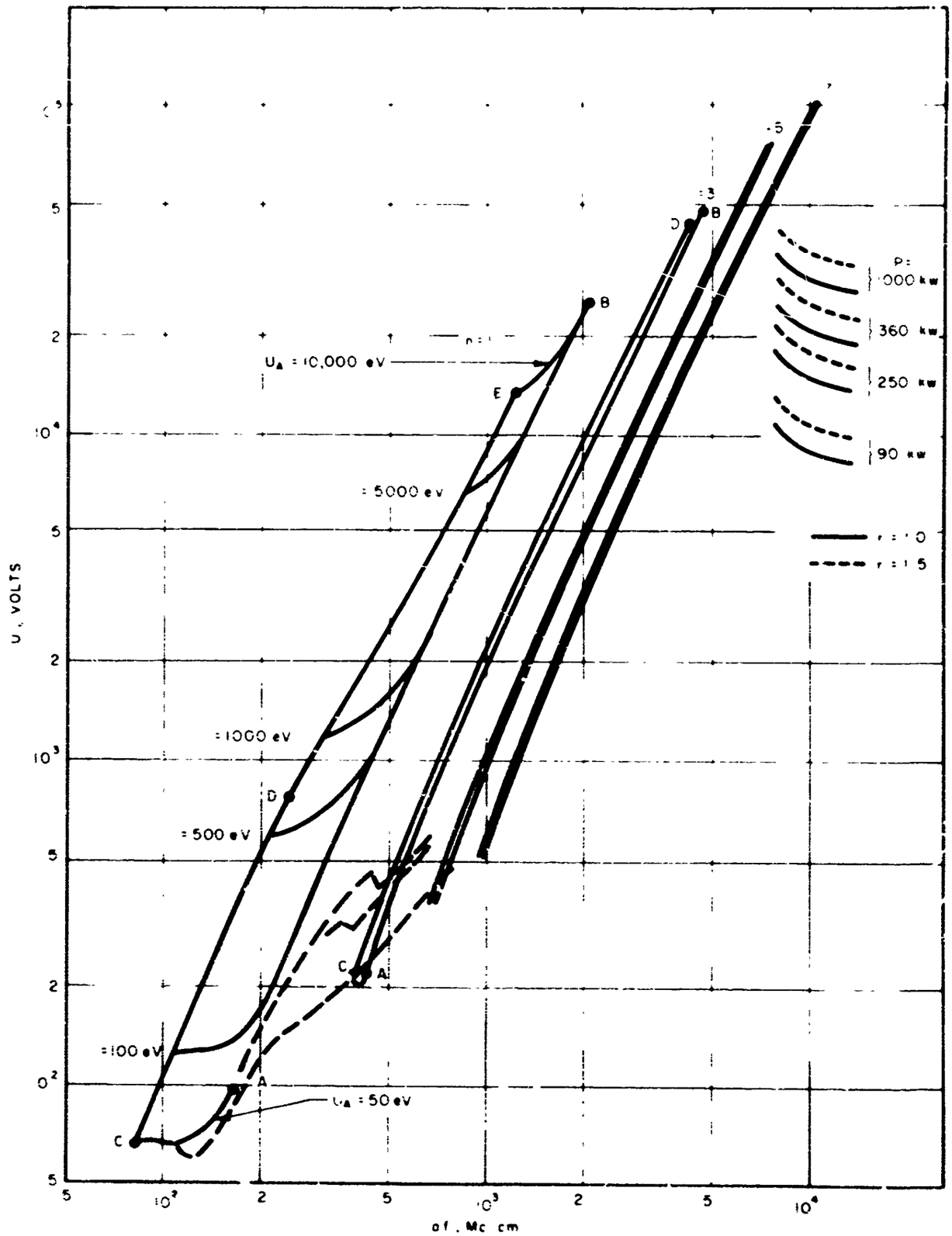

Figure 8. Existence Regions for the Multipactor Effect, Assuming U_s = 5 eV. Also Plotted are Loci of Waveguide Operating Points for Various Values of Incident Power P and Voltage Standing Wave Ratio r (see Section 5 of this Report) (from Zeitschrift für Physik, Band 175, 1963, p. 387)

$$n = 7: \quad U_e = 1.010 \times 10^{-3}(af)^2 - 0.2110(af)\sqrt{U_s} \tag{28c}$$

$$n = 9: \quad U_e = 0.792 \times 10^{-3}(af)^2 - 0.2113(af)\sqrt{U_s} \tag{28d}$$

$$n = 11: \quad U_e = 0.6483 \times 10^{-3}(af)^2 - 0.2115(af)\sqrt{U_s} \tag{28e}$$

$$\text{large } n: \quad U_e = \frac{7.143}{n} \times 10^{-3}(af)^2 - 0.2118(af)\sqrt{U_s} \tag{28f}$$

The critical starting amplitude as a function of af is represented in Figure 8 by the lines AB for the first few multipactor modes. The remaining boundaries of the existence regions for the multipactor effect are: 1) the lines CD determined by the phase stability condition expressed in Equation (18); 2) the lines DE determined by the condition governing electron return expressed in Equation (10); and 3) the lines EL and CA representing, respectively, upper and lower limits on electron impact energy which define, for any particular wall material, the range of impact energies over which the secondary emission ratio δ exceeds unity. All of the various parts of the boundaries of the existence regions must be found by numerical calculation, using relations implicity relating U_o to af. An explicit expression for voltage amplitude as a function of af can be obtained only for the portions AB of the boundary. It may be mentioned here that the portion DE of the boundary, determined by the condition (10) governing electron return, does not appear for the higher order modes for the range of impact energies considered in Figure 8, namely 50 eV to 10,000 eV. The sole condition governing the upper critical voltage amplitude is condition (18) governing phase stability.

Figure 8 clearly shows how the effective amplitude range rapidly diminishes for higher order multipactor modes. It is interesting to note that there is no overlapping of the various existence regions, such as was found by Hatch and Williams (Ref. 10), who started with the unfounded and incorrect assumption that the ratio of impact velocity to emission velocity is a constant.

The problem as defined here is a completely deterministic one. An electron upon being emitted will have its future course determined by the force of the electric field acting upon it. Hence, it can follow only one trajectory and not one of several, which would be implied if the existence regions for the various multipactor modes did indeed overlap.

To investigate the way in which the existence regions change for different assumed values of emission velocity, Krebs and Kossel (Ref. 15) have performed computations for the n = 1 and n = 3 modes, assuming emission velocities corresponding to 0, 5, and 10 eV. Their results are reproduced in Figure 9. The designations of the various portions of the boundaries are the same as those used in Figure 8. It can be seen that the regions corresponding to the three different emission velocities largely overlap for the n = 1 mode. This would mean that if the operating point were chosen within the overlap zone (e.g., for the regions computed in Figure 9, within the cross-hatched region corresponding to zero emission velocity, which region also lies within the existence regions for the 5 and 10 eV cases) then practically all electrons in the velocity distribution applicable to the secondary emission process would be effective in contributing to multipactor breakdown. However, the corresponding regions for the n = 3 mode diverge markedly for decreasing values of af. This fact again strongly suggests that breakdown in higher order modes is unlikely, since for the velocity distributions which occur in reality only a fraction of the emitted electrons would be effective in contributing to multipactor breakdown. The foregoing represents a feasibility argument rather than a rigorous demonstration, since the theory upon which the computations for the existence regions of Figure 9 were based assigns the same unique emission velocity to each successive electron emission process in the buildup of the multipactor effect.

Another interesting feature of the multipactor effect deserves to be mentioned here. According to the theory developed in Section 3 of this report, the impact energy of electrons participating in multipactor breakdown increases with

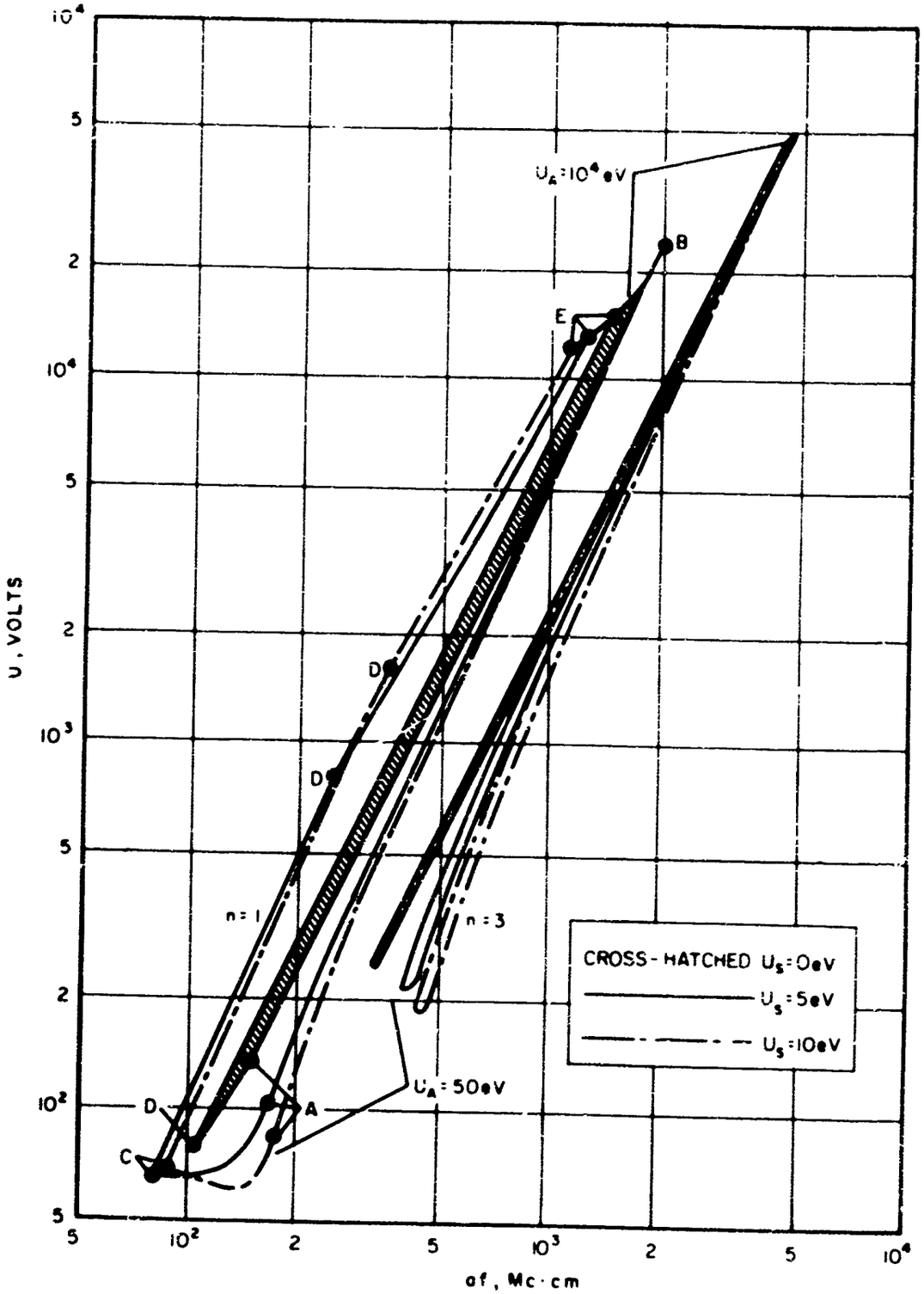

Figure 9. Existence Regions for the Multipactor Effect for Various Values of Emission Energy (from Zeitschrift für Physik, Band 175, 1963, p. 389)

increasing values of af. This is most clearly shown by the curves of Figure 8. Increasing the wall spacing a, for example, requires a higher voltage amplitude and yields a higher impact energy. To illustrate this point by means of a numerical example, suppose that 100 eV represents the impact energy above which the secondary emission ratio for the particular wall material used is greater than unity. Then, according to Figure 8, for values of (af) from 100 to about 200 Mc·cm, the n = 1 breakdown mode will indeed occur as soon as the voltage amplitude is raised to the point which yields an electron impact energy of 100 eV. However, for values of (af) above ~ 200 Mc·cm, the contours of constant impact energy show that electrons participating in multipactor breakdown will possess impact energies in excess of 100 eV. In fact, the impact energy increases very rapidly with (af), reaching 5,000 eV for a value of (af) of about 700 Mc·cm. Starting with a low value of voltage amplitude below the critical starting amplitude and increasing this value steadily, the secondary electrons which arrive at the opposite wall will have steadily increasing impact energies. If (af) > ~ 200 Mc·cm, breakdown will not occur when the impact energy reaches 100 eV. This can be explained by the fact that no phase focusing takes place for the corresponding values of β. In terms of the analysis of Section 3, the value of β is such that the argument of the arc cos function appearing in Equation (20) for the emission phase ϕ_s is not real. Therefore, in spite of the fact that some electrons reach the opposite wall with impact energies exceeding 100 eV, no breakdown occurs as yet because of the lack of phase focusing. This means that the secondary electrons produced upon impact and their descendants are largely lost by eventually returning to their plane of origin instead of crossing over to the opposite plane. This point constitutes another weakness of the theory of Gill and von Engel (Ref. 7) and Hatch and Williams (Ref. 9), who assume that breakdown will occur as soon as electrons begin to impact with a value of impact energy which yields a secondary emission ratio exceeding unity.

SECTION 5

EXPERIMENTAL VERIFICATION OF THE THEORY

Most of the papers dealing with the multipactor effect which have appeared in the literature and which are listed at the end of this report contain a discussion of experimental work performed under various conditions. Almost without exception, the breakdown was initiated between parallel plane electrodes contained in an evacuated chamber. In some investigations (Refs. 8 through 12) glass chambers were used; in other cases (Refs. 13, 14, and 15) microwave resonators were used. Apparently no one has yet used ordinary waveguide in an experimental investigation. The resonator investigations were confined to the n = 1 mode and showed excellent agreement with the theory of Krebs and Meerbach. In all cases, discrepancies between theory and experiment could be satisfactorily explained by a consideration of field fringing in the resonator gap where the breakdown was produced, by charge accumulating on the enclosing glass walls, and by space charge effects. The use of a resonator will, of course, substantially reduce the amount of power required to establish a certain voltage amplitude between parallel walls. The experimental work of Krebs and Meerbach is confined solely to the n = 1 mode. In Reference 15 Krebs and Kossel show how well their experimental results and the results of Hatch and Williams agree with the theory. They also show how Hoover and Smither in some unpublished work using a linear accelerator did indeed observe multipactor breakdown in higher order modes. This is apparently the only case known so far where a higher order breakdown mode has been observed experimentally.

In conclusion, it may be stated definitely that experimental measurements of multipactor breakdown conditions confirm with remarkable accuracy the theory of Krebs and Meerbach. This theory may, therefore, be used with a high degree of confidence in predicting breakdown possibilities in a practical system design that makes use of high power components operating at low gas pressures.

SECTION 6

SPECIAL CONSIDERATIONS APPLICABLE TO WAVEGUIDES

The theory of Section 3 may be used to predict breakdown conditions for rectangular waveguides operating at high power levels and low gas pressures. The well-known expression relating transmitted power P to peak electric field amplitude E_{max} at the center of a rectangular waveguide operating in the dominant TE_{01} mode is

$$\frac{P}{E_{max}^2} = 6.63 \times 10^{-4} ab\left(\frac{\lambda}{\lambda_g}\right) \tag{29}$$

where P is in watts, E_{max} is in volts per centimeter, the guide dimensions a (narrow dimension) and b (wide dimension) are expressed in centimeters, and λ and λ_g are, respectively, the free space wavelength and the guide wavelength. The peak voltage U_0 across the guide in volts is given by

$$\left.\begin{aligned} U_0 = E_{max}\, a &= \frac{\sqrt{P}}{\sqrt{6.63 \times 10^{-2}}} \sqrt{\frac{a}{b}} \sqrt{\frac{\lambda_g}{\lambda}} \\ &= 38.8\sqrt{\frac{a}{b}}\ \frac{\sqrt{P}}{\left[1 - \left(\frac{\lambda}{\lambda_c}\right)^2\right]^{1/4}} \end{aligned}\right| \tag{30}$$

where λ_c is the cutoff wavelength and is equal to 2b for the TE_{01} mode. This equation reveals that, for a fixed power level P, U_0 will remain essentially constant regardless of the waveguide band used, since changing bands will change a and b by the same factor, and since the operating wavelength may be chosen to be the same fraction of the cutoff wavelength λ_c.

Actually, not all of the standard EIA waveguide sizes have a and b in exactly the same ratio. The waveguides of this series have the ratio a/b = 0.5 with the following exceptions:

Waveguide Designation	WR 284	WR 187	WR 137	WR 112	WR 90	WR 42
Frequency Range (Gc)	2.60 to 3.95	3.95 to 5.85	5.85 to 8.20	7.05 to 10.00	8.20 to 12.40	18.00 to 26.50
Ratio a/b	0 472	0.466	0.453	0.443	0.444	0.405

Equation (30) shows that operating close to cutoff results in a high peak voltage U_0 for a given power level P. In order to minimize U_0 for a given P it is desirable to operate as far from cutoff as possible without, of course, permitting propagation in a higher order propagating waveguide mode. The latter restriction limits the value of the factor $\left[1 - (\lambda/\lambda_c)^2\right]^{1/4}$ to about 0.92 and hence is not significant since this value is quite close to the zero wavelength limit. Thus, for comparable operation (relative to cutoff) in any waveguide band, the peak voltage will be at least

$$U_0 = 38.8 \times \sqrt{.472} \times \sqrt{P}/0.92 = 29.0\sqrt{P} \qquad (31)$$

where, again, P is in watts and U_0 is in volts. Figure 10 presents this relation graphically. The foregoing discussion has disregarded the possibility of a voltage standing wave ratio existing in the waveguide. The peak voltage U_0 will be increased by the factor $1 + |\Gamma|$ where $|\Gamma|$ is the magnitude of the voltage reflection coefficient and is related to the voltage standing wave ratio r by the equation

$$|\Gamma| = \frac{r - 1}{r + 1} \qquad (32)$$

Curves for several values of r are also plotted in Figure 10.

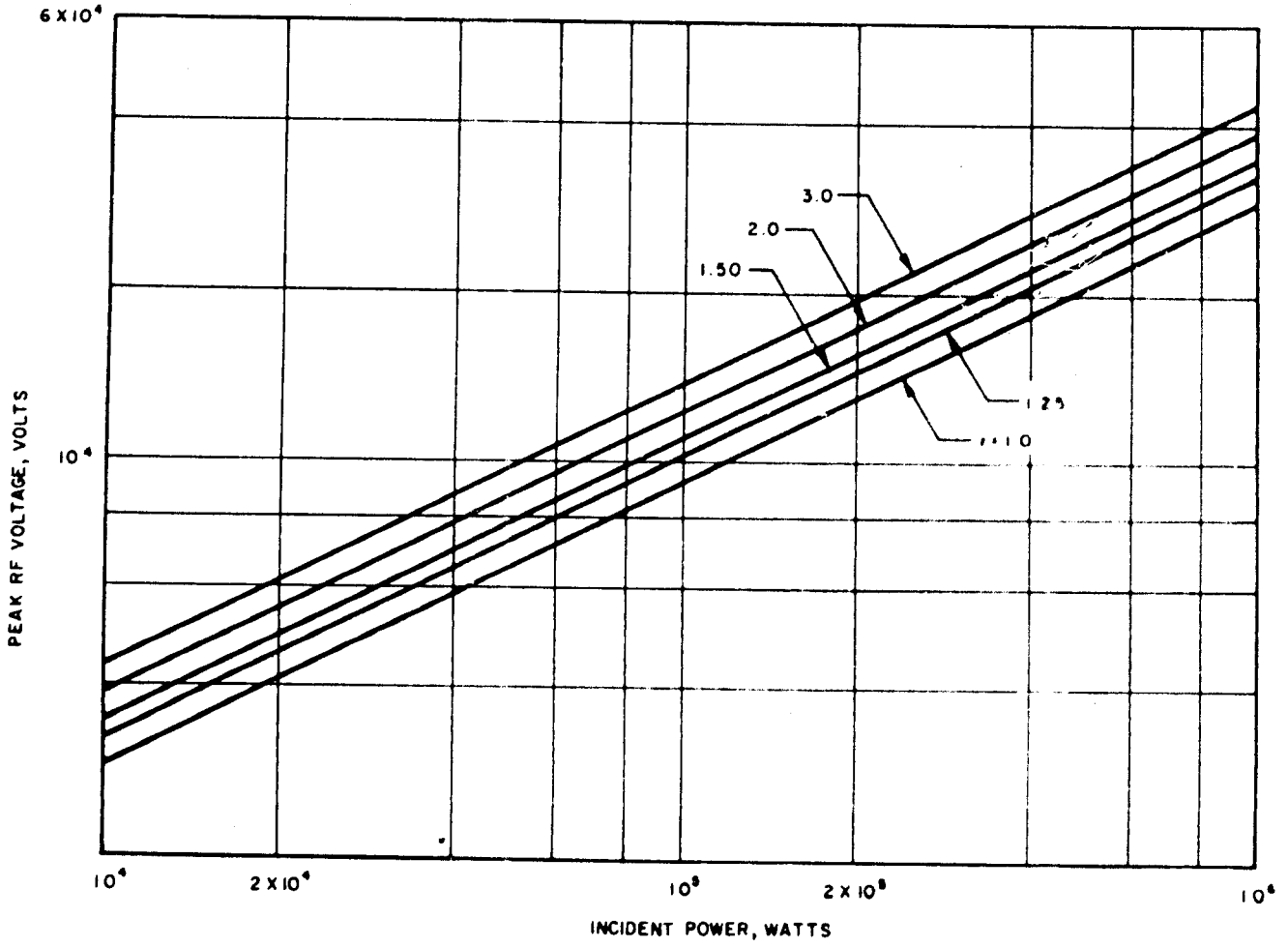

Figure 10. Peak Voltage Across Rectangular Waveguide vs Incident Power ($f/f_c = 1.89$)

The value of the product af will also be approximately constant for all waveguide bands. Expressed in units of Mc · cm, this value will range from about 1.14×10^4 to about 1.43×10^4 for the various standard waveguide sizes, computed in each case for the highest practically usable frequency For standard X-band guide (WR 90) the highest value of af is 1.26×10^4, for f = 12.40 Gc. At f = 8.20 Gc, the value of af is 0.83×10^4. It is interesting to observe the effect of varying frequency over the usable waveguide band for a particular waveguide, holding incident power constant. The loci of operating points for standard X-band guide are plotted in Figure 8 with the various multipactor mode existence regions. Corresponding loci for other sizes of waveguide will practically coincide with these loci. Several values of voltage standing wave ratio and incident power are assumed. It can be clearly seen from Figure 8 that in order to minimize the danger of multipactor breakdown it is very desirable to operate near the upper end of the usable waveguide frequency band. In normal waveguide operation it is only the higher order multipactor breakdown modes which may pose a problem. Of course, only extremely high power levels need cause any concern.

The divergence of the multipactor breakdown regions for various assumed values of secondary emission velocity was discussed in Section 4 and is illustrated in Figure 9. Thus, in addition to severely restricting the required range of voltage amplitude, going to a higher order mode has the additional effect of eliminating from the avalanche breakdown process all but a fraction of the secondary electrons that have emission velocities spread over a certain range.

To gain some idea of the order of the breakdown mode involved in waveguide multipactor breakdown, a simple numerical example can be given here. Suppose it is required to transmit a peak power level of 250 kw. Waveguide size is not important. According to Equation (31), peak voltage across the guide will be 14,500 volts for standing wave ratio r = 1 or 17,400 volts for

$r = 1.5$. Assuming an emission energy of 5 eV and letting $af = 1.14 \times 10^4$ as discussed in Section 6, then Equation (28f) shows that, for $r = 1.5$, the peak voltage amplitude will lie in the theoretical breakdown region for $n = 41$! Even assuming $r = 1.0$ and $af = 0.83 \times 10^4$, Equation (28f) shows that the appropriate breakdown mode would be the $n = 23$ mode! Changing the assumed transmitted peak power level to 500 kw, the foregoing two results become $n = 31$ and $n = 17$, respectively. Of course, breakdown modes of such high order will have extremely small voltage amplitude ranges for breakdown. Clearly, for rectangular waveguides of ordinary cross section, multipactor breakdown is extremely unlikely.

Because of the sinusoidal voltage amplitude distribution across the broad dimension of a waveguide, it is not sufficient to locate the waveguide operating point (based upon the peak value of voltage amplitude) between the separated breakdown modes of Figure 8, since there will be operating points for somewhat lower amplitudes off the guide center, which will in general lie in the existence regions for one or more of the higher order breakdown modes. The operating conditions must be chosen so that the operating points for the peak voltage amplitude (at the guide center) and all lower amplitudes are free of the existence regions for the multipactor breakdown modes in the chart of Figure 8.

SECTION 7

CONCLUSIONS

The analysis presented in this report has shown that multipactor breakdown can occur in various modes, each characterized by an electron transit time equal to a certain odd number of half cycles of the propagating energy. The results have been presented in several graphical forms. The only simplification made in obtaining the breakdown conditions has been the assumption of a unique emission velocity for the secondary electrons, rather than a velocity distribution. The analysis, originally due to Krebs and Meerbach, leads to more realistic results than do previous analyses that made use of additional simplifying assumptions. Experimental measurements have confirmed the quantitative predictions of this theory with remarkable accuracy. The theory can, therefore, be used with a high degree of confidence in predicting multipactor breakdown possibilities.

In general, breakdown in the high order breakdown modes is difficult to achieve because of the much narrower ranges of values of voltage amplitude required for breakdown. These ranges of values are so restricted that, to a large extent, they do not even overlap for different assumed values of emission velocity. This makes breakdown in the higher order modes even less likely because of the velocity distribution of the secondary electrons.

The foregoing remarks apply to the problem of transmitting high power levels through a rectangular waveguide at low gas pressure. Because of the relationship between waveguide size and operating frequency, the operating point is so located in the breakdown charts that only the higher order breakdown modes are of concern. It appears that breakdown is quite unlikely in this case because of the high order of the mode involved and the exceedingly restricted range of voltage amplitude required for breakdown.